Molecular insights into the formation of drug-polymer inclusion complex

Binbin Liu[†,a], Changrui Li[†,b], Ziqiao Chen[a], Xiao Ou[a], Shuting Li[a], Ao Li[a], Pin Chen[*, c], Ming Lu[*, a]

Abstract: Drug-polymer inclusion complex (IC) has been viewed as a novel solid form of drugs for property modification. Nonetheless, our understanding of the formation mechanism remains limited. This work aims to provide insight into the molecular processes governing the structural construction of carbamazepine (CBZ) and griseofulvin (GSF) channel-type ICs in the presence of guest polymers. Leveraging microdroplet melt crystallization, we successfully unveiled the single-crystal structures of these ICs, enabling theoretical analysis. Our investigation, which encompasses structural analysis, density functional theory calculations, and molecular dynamics (MD) simulations, elucidates the disparity between CBZ and GSF channels in terms of their autonomy in the absence of guest polymers. CBZ molecules can spontaneously assemble into stable channel structures independently, capitalizing on their unique mortise-tenon architecture and robust π…π interactions. In contrast, GSF channels lack sufficient support from weak Cl…O and C-H…π intermolecular interactions and necessitate the insertion of guest molecules to stabilize their structures. Regardless of the structural reliance on guest polymers, channel size is determined by the size, shape, and conformation of the host molecules, as well as intermolecular interactions. Interestingly, while the eleven structurally determined drug-polymer ICs adopt diverse approaches to construct channel structures, their channel sizes consistently fall within a narrow range of 3.86-5.18 Å, slightly larger than the radial diameter of the guest polymers (2.83-3.50 Å). Consequently, we propose that a crucial prerequisite for the formation of drug-polymer ICs is that the host molecules have the capacity to self-assemble into a porous structure with accommodating channels for guest polymers. Additionally, our results confirm the efficacy of microdroplet melt crystallization in rapidly synthesizing drug-polymer ICs and cultivating their single crystals of high quality and sufficient size. This achievement overcomes the challenges associated with structure elucidation and promises to promote further research into the formation mechanism of drug-polymer ICs. We anticipate that these findings will inspire continued exploration of this novel solid form, facilitating theoretical predictions and practical applications in pharmaceutical development.

1. Introduction

Oral formulations make up roughly 90% of the global market share for human pharmaceuticals, with the majority being developed in solid dosage forms[1]. The properties of drugs in solid dosage forms, such as stability, tabletability, dissolution, and even absorption, can be tuned by choosing different solid-state forms. These options include one-component systems (e.g. amorphous form, polymorph, and salt) and multiple-component systems (e.g. solvate, cocrystal, and inclusion complex (IC))[2].

Conventional IC typically involves a two-component system where the drug molecules are enclosed within cyclodextrin cavities[3]. This cyclodextrin-drug IC has shown the capability to enhance drug solubility[4], leading to the development of commercial products like Allidex®, Geodon®, and Cardiotec®[5].

In 1983[6], Suehiro *et al*. reported a groundbreaking concept by describing an innovative pharmaceutical IC. In this IC, urea, typically used as a medication for skin disease, served as the host molecule, arranging itself into a channel-type crystal structure to encapsulate the guest polymer, polyethylene glycol (PEG). Although the idea of creating small-molecule host - macromolecule guest systems had been under exploration since the 1960s, examples like perhydrotriphenylene[7] and tris(o-phenylenedioxy) cyclotriphosphazene[8], the urea IC marked a significant advancement in pharmaceutical applications[6, 9]. After a span of 23 years, the second instance of a drug-polymer

[a] *School of Pharmaceutical Sciences, Sun Yat-sen University, Guangzhou 510006, China. E-mail: luming3@mail.sysu.edu.cn*
[b] *Guangzhou Zhixin High School, 152 Zhixin South Road, Guangzhou 510080, China*
[c] *National Supercomputer Center in Guangzhou, School of Computer Science and Engineering, Sun Yat-sen University, Guangzhou 510006, China. E-mail: chenp85@mail.sysu.edu.cn*
† These authors contributed equally.
* These authors jointly supervised this work.
Electronic Supplementary Information (ESI) available: CCDC 2265934 2265556 2265555 2121359 2121358 2121357. For ESI and crystallographic data in CIF or other electronic format see DOI: 10.1039/x0xx00000x.

IC was disclosed in a patent by Calvin CC Sun and collaborators[10]. In this case, the host molecule was mavacoxib, a non-steroidal anti-inflammatory drug, while PEG served as the guest polymer. Recent research has unveiled an expanding repertoire of drugs capable of forming ICs with guest polymers. Notable examples include griseofulvin (GSF, 2014, an antifungal drug)[11, 12], diflunisal (DIF, 2016, an anti-inflammatory drug)[13-15], dapsone (DAP, 2018, an antileprotic drug)[16], carbamazepine (CBZ, 2019, an antiepileptic drug)[17, 18], finasteride (2020, used for treating androgenetic alopecia)[19] and nevirapine (NIV, 2021, an anti-HIV drug)[20]. Furthermore, beyond the hydrophilic PEG, guest polymers have expanded to include hydrophobic polymers, such as poly(ε-caprolactone) (PCL)[15], and amphipathic polymers, exemplified by PEG-b-PCL[14].

Compared to cyclodextrin, polymeric excipients offer a greater degree of flexibility in terms of adjustability, including factors like chemical structure and molecular weight. As a result, drug-polymer IC, where the drug acts as the host and the polymer as the guest, provides a more versatile means of regulating the release behavior of drug. This versatility opens the door to a broader range of potential applications, surpassing the conventional cyclodextrin-drug IC approach. For instance, when incorporating hydrophilic PEG into channels designed for GSF, it is possible to enhance both the dissolution and solubility of GSF[12]. Furthermore, by adjusting the molecular weight of PEG, it becomes feasible to finely tune the dissolution profiles of GSF within PEG-based ICs[12]. In the case of CBZ, PEG-encased ICs exhibit faster dissolution, while PCL-inserted ICs exhibit similar dissolution rates but offer improved physical stability against phase transformation into CBZ hydrate when exposed to aqueous solutions in comparison of CBZ Form II, the raw material [18]. DIF, on the other hand, can be formulated as a PCL-based IC to achieve sustained release, making it a promising approach for controlled drug delivery[15]. In the agricultural sector, urea ICs involving degradable polyesters have been explored as an eco-friendly strategy for extending the release of fertilizers[21]. As a result, the concept of drug-polymer ICs has emerged as a novel solid form for customizing the properties of APIs[22].

However, despite the fact that four decades have passed since the introduction of the first drug-polymer IC, our knowledge remains limited and only eight APIs known to form such complexes[6, 10, 11, 13, 16, 18-20]. What's more, half of these complexes have not yet had their structures fully determined[10, 12, 13, 18, 19]. The challenge in identifying their structures presents a significant obstacle to comprehending the mechanisms underlying their formation, thus impeding our ability to make informed theoretical predictions. As a result, the screening of drug-polymer ICs continues to depend largely on a trial-and-error approach.

In the quest for identifying the structures of ICs, single-crystal structure determination stands as the gold standard. Although three dimension electron diffraction has demonstrated its utility in recent years for structure determination[23], single-crystal X-ray diffraction (SCXRD) remains the predominant method for structure determination in most laboratories. However, one of the key challenges in this process is the successful growth of a single crystal with both adequate size and quality, a task that often proves to be quite challenging. This difficulty in obtaining suitable single crystals may be a contributing factor to the fact that half of the previously reported drug-polymer ICs still lack known structures[10, 12, 13, 18, 19], including cases like CBZ-polymer[18] and GSF-PEG[11] ICs, among others. Recently, a new approach has been developed involving a melt microdroplet strategy designed to expedite the growth of single crystals from melts[24]. This innovative strategy has shown significant promise in accelerating fundamental research in pharmaceutical solid-state chemistry, encompassing areas such as polymorphism[25-27] and cocrystals[28] of clinical drugs. In this study, this strategy is applied to the task of identifying the structures of drug-polymer ICs, with the aim of shedding light on the mechanisms underlying their formation.

In this work, we focused on two clinical drugs: CBZ and GSF, as depicted in **Figure 1**. Both of these drugs are poorly water-soluble, which makes them common model drugs for investigating various strategies to enhance the solubility[29]. Notably, recent studies have reported the formation of channel-type ICs with linear polymers for both CBZ and GSF, as confirmed through nuclear magnetic resonance (NMR) and powder X-ray diffraction (PXRD)[11, 17, 18]. However, the crystal structures of these complexes have remained elusive. One critical and intriguing difference between the CBZ and GSF IC systems is their distinct reliance on guest molecules. The CBZ channel structure can form in the absence of guest molecules, which is referred to as a "true polymorph" of Form II[30]. This true polymorph of CBZ shares its structure with CBZ solvates and ICs[30], and it can be produced through spontaneous crystallization from solutions in ethanol and ethyl acetate, as well as by dehydrating its dihydrate at 20°C. In contrast, as far as our knowledge goes, GSF channels only seem to emerge in the presence of guest solvents or polymers. The desolvation of the GSF-acetonitrile solvate, which is isostructural to GSF-PEG ICs, leads to the formation of GSF Form I rather than the GSF channel structure. We attempted to synthesize pure GSF channels by seeding GSF-PEG ICs into molten GSF but obtained GSF Form V instead[31]. This intriguing difference in their behavior highlights the complexity of these inclusion complexes and the challenges associated with their structural determination.

Our objective in this study is to uncover the molecular mechanisms underlying the distinct dependencies of GSF and CBZ ICs on guest polymers. By combining structural elucidation and theoretical calculations, we aim to pinpoint the factors that contribute to this differentiation. This endeavor will not only shed light on the reasons behind this contrast but also provide valuable insights into the formation mechanisms of drug-polymer ICs.

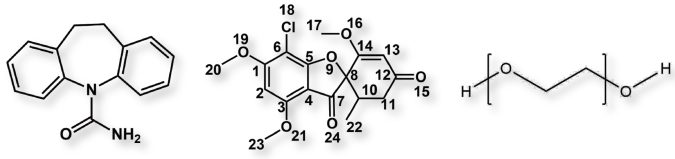

Figure 1. Chemical structures of CBZ, GSF, and PEG.

2. Experimental Section

2.1 Materials

CBZ (purity > 99.5%, Form I), GSF (purity > 99.5%, Form I), PEG (M_w = 6000 and 8000 g/mol), PCL(M_w = 36000 and 45000 g/mol), and PTHF (polytetrahydrofuran, M_w = 2000 g/mol) were purchased from Aladdin (Shanghai, China). poly(1,4-butylene adipate) (PBA, M_w = 12,000 g/mol) and poly(ethylene succinate) (PES, M_w = 10,000 g/mol) were purchased from Aldrich (St. Louis, USA). Polyvinylpyrrolidone (PVP, M_w = 50,000 g/mol), poly(1-vinylpyrrolidone-co-vinylacetate) (PVP VA, M_w = 45,000 g/mol), and PEG 6000-vinylcaprolactam-vinyl acetate grafted polymer (Soluplus, M_w = 118,000 g/mol) were kindly supplied by BASF SE (Ludwigshafen, Germany). Hydroxypropyl-methylcellulose acetate succinate (HPMCAS HF, M_w = 75,100 g/mol) was kindly supported by Ashland (Wilmington, USA) (**Figure S1**).

2.2 Preparation of IC samples

Physical mixtures of drug and polymer (50:50, w:w) were prepared by accurately weighing the samples into a mortar and manually grinding. Then, the samples were melted using a Linkam hot stage (THM S600, Waterfield, UK) equipped with a Nikon polarized optical microscope (POM, Nikon Eclipse LV100N POL, Nanjing, China), followed by holding at 85 °C and room temperature to yield GSF-polymer and CBZ-polymer ICs, respectively. PEG 8000 was used in GSF-PEG IC, while PEG 6000 was used in CBZ-PEG IC.

2.3 PXRD

PXRD patterns of samples were obtained using a Rigaku X-ray diffractometer (SmartLAB, Tokyo, Japan) with λ = 1.542 Å. The scan speed is 6°/min.

2.4 Growth of single crystals

Single crystals were produced by applying the melt microdroplet method using a hot-stage microscope. The melting and cultivation temperatures and the POM images of single crystals are listed in **Table S1** and **Figure S2**. For GSF-PEG and GSF-PES ICs, it is difficult to grow single crystals by melt microdroplet strategy because they always transform to Form V upon melting. Fortunately, as they grew at 85 °C for 120 min (GSF-PEG IC) or 90 °C for 60 min (GSF-PES IC), the edge of their spherulites grew as single crystal morphology. We cut off a block of single crystal parts with a blade for the SCXRD test.

2.5 SCXRD and structure elucidation

Diffraction signals were collected using single crystals cultivated from melts with a Rigaku diffractometer (XtaLAB Synergy, Wroclaw, Poland) equipped with an Oxford Cryosystems low-temperature device with Cu Kα radiation (λ = 1.54184 Å). Cell refinement and data reduction were performed using CrysAlisPro 1.171.39.46.25 software[32]. Crystal structures were solved by intrinsic phasing methods using SHELXT[33] and refined by full-matrix least-squares using SHELXL[34] using Olex 2. The calculated PXRD patterns and structure analysis were performed using Mercury 2020.3.0.

2.6 Simulation methods

We performed all the calculations by using the Vienna Ab initio Software Package (VASP)[35] code with the Perdew–Burke–Ernzerhof (PBE) functional[36] and the frozen-core all-electron projector augmented wave (PAW) model[37]. The bulk structures of CBZ and GSF were obtained from the Cambridge structural database (CSD). We relaxed the bulk structures using the plane-wave expansion of the electronic wave functions with a 450 eV plane wave cutoff energy. The Brillouin zone of the unit cell was sampled by Gamma grids by a k-point grid of 10 × 3 × 3. The convergence criterion for the electronic self-consistent iteration was 10^{-5} eV and set 0.01 eV/Å for the force components during geometry optimizations. We further performed ab-initio molecular dynamics simulations by implementing optimized structures to study the thermodynamic stability of simulation systems. The simulations based on the Nose-Hoover thermostat algorithm were carried out for 30,000 steps with a time step of 1 fs (total 30 ps) under the NVT ensemble.

The binding energy per molecule ($E_{binding}$)is estimated using the following equation:

$$\Delta E_{binding} = \frac{[E_{IC} - (E_{drug} + E_{polymer})]}{N} \quad (1)$$

Where E_{IC} is the energy of drug-polymer IC, E_{drug} and $E_{polymer}$ refer to the energy of drug molecules and PEG, respectively. All energy values were estimated by density functional theory (DFT) calculation. N is the total number of drug molecules in the crystal structure. The binding energies were normalized by dividing them by N for comparison among different drug-polymer ICs.

The cohesive energy per molecule ($\Delta E_{cohesive}$) is calculated using the equation:

$$\Delta E_{cohesive} = \frac{[E_{IC\ removing\ polymer} - N \times E_{drug}]}{N} \quad (2)$$

Where $E_{IC\ removing\ polymer}$ represents the energy of drug-polymer IC after removing polymer chains.

The channel size was calculated using the open-source software Zeo++[38].

3. Results and discussion

3.1 Structure identification of three CBZ-polymer ICs

We successfully grew single crystals of three known CBZ ICs using the melt microdroplet strategy, as shown in **Figure S2 a-c** and **Table S1**. The crystal structures of these ICs were determined by SCXRD, as presented in **Figure S2** and **S3**. The simulated PXRD patterns closely match the experimental PXRD patterns, confirming the accuracy of the structures (**Figure S4**). The crystallographic parameters for these ICs are listed in **Table 1**, indicating that three CBZ ICs are isostructural with CBZ Form II[30] and CBZ monohydrate[39]. We take CBZ-PEG IC as an example to illustrate the structure of CBZ-polymer ICs. It crystallizes in a monoclinic crystal system with a space group of $R\bar{3}$. The lattice parameter are a=34.7897(11), b=34.7897(11), and c=5.2486(2) and γ = 120°. In the structure, all CBZ molecules form dimers through C=O…H-N hydrogen bonds, as shown in **Figure 2a**. When viewed along the c-axis, six CBZ dimers aggregate into a ring structure as depicted in **Figure 2a**. These rings stack in parallel along the c-axis to create a channel, as evident in **Figure 2b-c**. Additionally, **Figure 2d** demonstrates the presence of π-π interactions between the CBZ aromatic rings along the c-axis. The center-of-mass distance between two parallel aromatic rings (z) measures 5.253 Å, and the distance between these rings (d) is 4.031 Å. The angle θ between d and z is 39.88°. The π-π interactions play a crucial role in strengthening the stacking of the aromatic rings, thereby enhancing stability of the channel structure. These stable channels allow linear polymer chains to be inserted through them, forming the IC structure.

Table 1 Crystallographic parameters of CBZ polymorph II, CBZ hydrate, and CBZ-polymer ICs.

	Form II[a]	Hydrate	CBZ-PEG IC	CBZ-PCL IC	CBZ-PTHF IC
Yr. discov.	2007[30]	2017[39]	2021[18]	2021[18]	2019[17]
Methods [ref]	SC	SC	MC	MC	MC
Yr. str. solved,	2007[30]	2017[39]	this work	this work	this work
Methods [ref]	SCXRD	SCXRD	SCXRD	SCXRD	SCXRD
CCDC No.	1121423	1494538	2265934	2265556	2265555
Temp., K	283-303	183	100	100	100
Cryst. syst.	trigonal	trigonal	trigonal	trigonal	trigonal
Space group	$R\bar{3}$ (148)	$R\bar{3}$ (148)	$R\bar{3}$ (148)	$R\bar{3}$ (148)	$R\bar{3}$ (148)
a, Å	35.454(3)	35.2832(9)	34.7897(11)	34.9833(14)	34.9429(12)
b, Å	35.454(3)	35.2832(9)	34.7897(11)	34.9833(14)	34.9429(12)
c, Å	5.253(1)	5.20165(13)	5.2486(2)	5.2078(2)	5.2235(2)
α, °	90	90	90	90	90
β, °	90	90	90	90	90
γ, °	120	120	120	120	120
Cell volume, Å^3	5718.32	5608	5501.43	5519.59	5523.45
Z, Z'	18, 1	18, 1	18, 1	18, 1	18, 1
ρ, g/cm^3	1.235	1.275	1.284	1.279	1.279
R factor, %	6.90	4.74	4.25	5.31	4.83

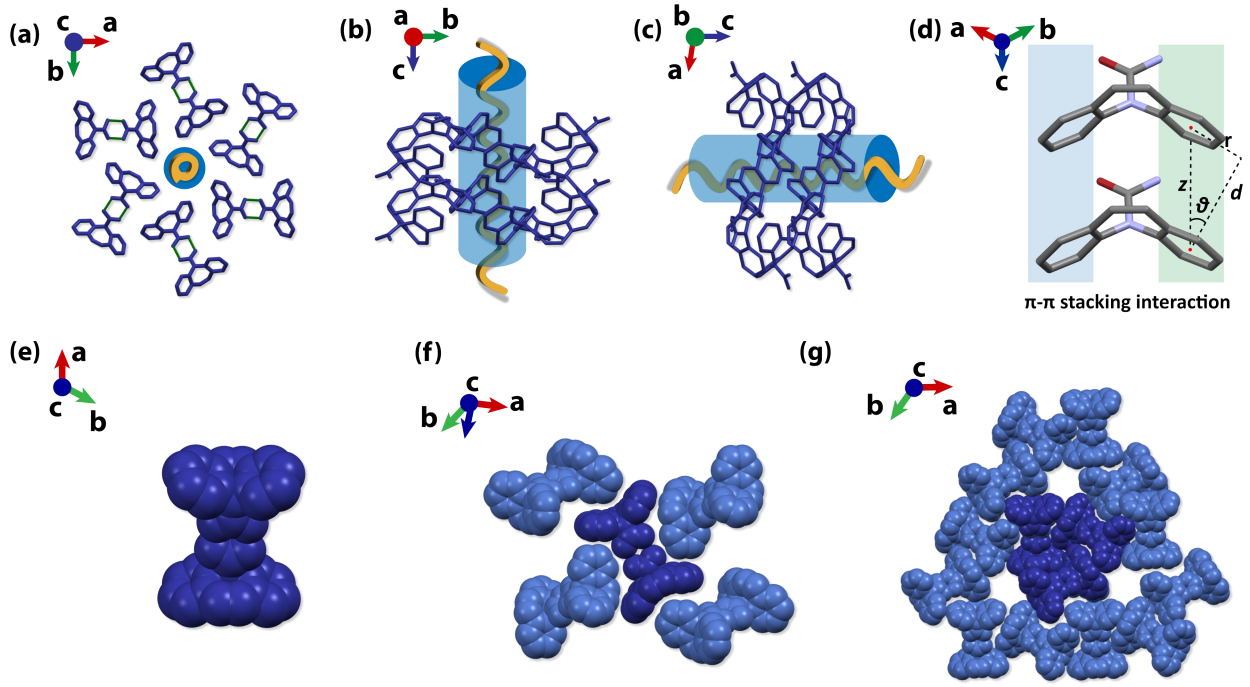

Figure 2. Crystal structure of CBZ-PEG IC. (a) Crystal packing viewed along the c-axis. (b) Crystal packing viewed along the a-axis. (c) Crystal packing viewed along the b-axis. (d) π-π stacking between CBZ molecules. (e) CBZ dimer is connected by two hydrogen bonds. (f) Mechanical lock among CBZ dimers. (g) Channel structure formed by the mechanical lock of dimers. PEG chains were removed due to serious disorder and are represented by an orange curve. The light blue cylinder is used to represent the channel in the crystal structure. The IC structures showing PEG and other polymers are given in **Figure S3**.

3.2 Structure elucidation of GSF-PEG IC

We successfully determined the structure of GSF-PEG IC using a single crystal cut from the edge of spherulite grown at 85 °C for 120 min (**Figure S2**). The results indicated that GSF-PEG IC crystallizes in a $C2$ space group and a monoclinic crystal system with similar crystallographic parameters with GSF-acetonitrile solvate: a = 11.6874(10) Å, b = 8.6513(7) Å, c = 20.205(2) Å, β = 98.641(9) ° (shown in **Table 2**). As shown in **Figure 3a-d**, the benzofuran ring is nearly paralleled to the b-

axis and connects to neighbors *via* Cl…O interactions (Cl…O24 = 3.359 Å for carbonyl oxygen and Cl…O21 = 3.261 Å for oxygen in methoxy) to form a line along *b*-axis (**Figure 3b**). The cyclohexatriene of the GSF molecule is nearly perpendicular to the benzofuran ring, and thus, a C22-H…π (3.107 Å) interaction forms between the methyl group on the cyclohexenone ring and the centroid of the phenyl group of the neighboring molecule along *c*-axis (**Figure 3d**), which connects two lines. As viewed along the *a*-axis, every four molecules form a rectangle-shaped channel by four Cl…O bonds (**Figure 3d**) and four C-H…π interactions. In previous work, the structure of GSF-PEG IC was considered to be isostructural with GSF-nitroethane (1:1) solvate through indexing the powder X-ray diffraction pattern[11]. In this work, the single-crystal structure of GSF-PEG IC is elucidated and found to be isostructurally related to the GSF-acetonitrile solvate (**Table 2**).

To test the efficiency of melt crystallization in IC screening, we attempted to synthesize GSF ICs with other two linear polymers, PBA and PES (shown in **Figure S1**), as guest polymers using melt crystallization. The polycrystals spontaneously nucleating from melts were used as seeds to grow single crystals from melt for structure elucidation (**Table S1** and **Figure S2d-h**). The SCXRD results indicated that both PBA and PES can form GSF-polymer IC and the two novel ICs are isostructural with GSF-PEG IC (see **Table 2** and **Figure S6**). This highlights the efficiency and convenience of melt crystallization as a valuable method in drug-polymer IC research. The successful structure determination opens up avenues for deeper exploration into the mechanisms behind the formation of these ICs.

Table 2. Crystallographic parameters of GSF-acetonitrile solvate and GSF-polymer ICs.

	GSF-acetonitrile solvate	GSF-PEG IC	GSF-PBA IC	GSF-PES IC
Yr. discov.	2014[31]	2014[11]	this work	this work
[ref]	SC	MC	MC	MC
Yr. str. solved,	2014[31]	this work	this work	this work
Method[a] [ref]	SCXRD	SCXRD	SCXRD	SCXRD
CCDC No[a]	924889	2121359	2121358	2121357
Temp., K	110	100	100	100
Cryst syst	monoclinic	monoclinic	monoclinic	monoclinic
Space group	*P*21 (4)	*C*2 (5)	*C*2 (5)	*C*2 (5)
a, Å	11.783(2)	11.6874(10)	11.74660(10)	11.6870(3)
b, Å	8.5387(17)	8.6513(7)	8.63920(10)	8.6507(2)
c, Å	19.297(4)	20.205(2)	20.5457(2)	20.4998(7)
α, °	90	90	90	90
β, °	96.03(3)	98.641(9)	98.8120(10)	99.412(3)
γ, °	90	90	90	90
Cell volume	1930.76	2019.76	2060.39	2044.64
Z, *Z*'	4, 2	4, 1	4, 1	4, 1
ρ, g/cm^3	1.355	1.345	1.137	1.146
R factor, %	5.56	7.86	4.44	4.34

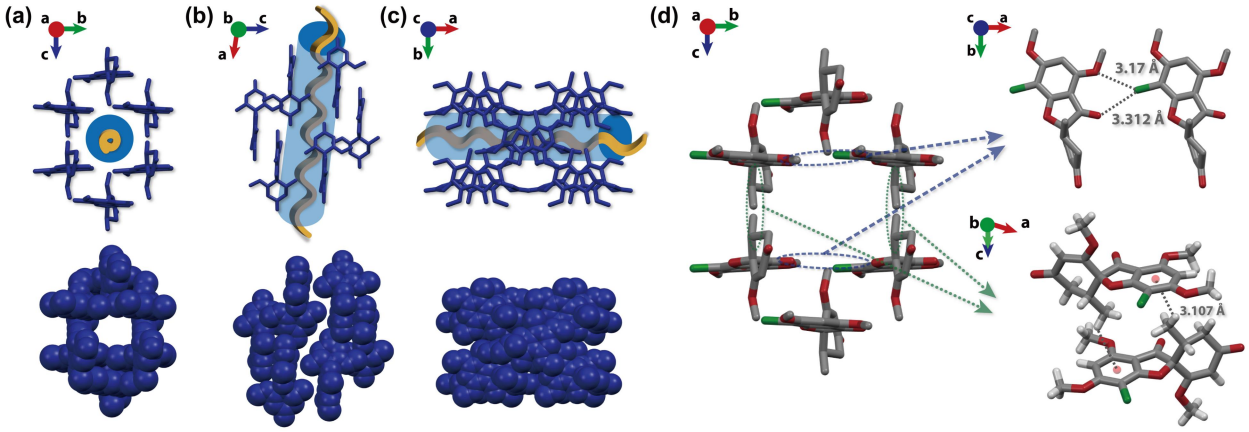

Figure 3. Crystal structure of GSF-PEG IC. (a) Crystal packing viewed along the *a*-axis. (b) Crystal packing viewed along the *b*-axis. (c) Crystal packing viewed along the *c*-axis. (d) Cl…O and C-H…π interaction that maintains the channel structure, where the carbon, chlorine, oxygen, and hydrogen atoms are marked in grey, light green, red, and white, respectively, and the centroid of the benzene ring is marked in light red. PEG chains were removed due to serious disorder and represented by a yellow curve. A light blue cylinder is used to represent the channel in the crystal structure. The IC structures showing PEG and other polymers are given in **Figure S5**.

3.3 Why can CBZ channels independently exist in the absence of guest polymers, but GSF channels cannot?

The notable difference between CBZ-polymer and GSF-polymer ICs lies in the fact that CBZ molecules can self-assemble into a channel structure independently in the absence of guest molecules (as true polymorph II), whereas GSF channels only take shape when polymers are introduced. To understand why these two IC systems exhibit different dependencies on polymers, we aim to address this question by conducting structural analyses and theoretical calculations.

The construction of channels in CBZ and GSF ICs differs significantly. In the case of CBZ channels, the structure is composed of bone-shaped CBZ dimers. Here, the N-H…O=C double hydrogen bonds connect two CBZ molecules, creating the "diaphysis". The two dibenzazepine rings serve as the "epiphysis" as illustrated in **Figure 2e**. These bone-shaped CBZ dimer features both convex and concave parts. The convex parts consist of four phenyl rings, while

the concave parts include a "diaphysis" site and two V-shaped dibenzazepine rings. These structural elements complement each other well. As illustrated in **Figure 2f** and **Movie S1**, each CBZ dimer mechanically interacts with four neighboring dimers. For the centrally positioned dimer, the "diaphysis" site accommodates a phenyl ring from the adjacent dimer on both the left and right sides and the two V-shape dibenzazepine rings each fit a phenyl ring of the neighboring dimers. This unique molecular conformation allows the CBZ dimers to be securely locked together, akin to the mortise and tenon joints often used in wooden architecture. Each dimer is stacked with others through π-π stacking interactions along the c-axis, forming a stable column. Six such columns are mechanically locked together through the mortise and tenon joints, culminating in the formation of a straight channel. These channels are interconnected in a similar manner, generating a porous structure, as depicted in **Figure 2g**. The presence of both mortise-tenon joints and strong π-π stacking interactions contributes to the exceptional stability of the CBZ channel structure. This explains why CBZ channels can spontaneously nucleate from solutions as polymorph II, even in the absence of guest molecules, despite their lower density (1.235 g/cm3 for CBZ Form II) compared to other true polymorphs (1.339 g/cm3 for Form I, 1.347 g/cm3 for Form II, 1.296 g/cm3 for Form IV, and 1.296 g/cm3 for Form V)[40, 41]. Furthermore, the CBZ channel structure remains stable even after the removal of guest solvent molecules (desolvation[42]). Conversely, GSF channels rely on weak Cl…O bonds and C-H…π interactions, as shown in **Figure 3e**. These weak interactions are insufficient to provide structural stability. Consequently, neat GSF channels cannot exist independently once the guest molecules are removed[31]. Therefore, the presence of guest molecules is essential for stabilizing GSF channels.

With the successful determination of crystal structure, we proceeded to conduct DFT calculations and molecular dynamics simulations to validate the mechanisms we discussed above. Given that PEG is the sole excipient approved by the U.S. food and Drug Administration for pharmaceutical use,[43] we opted to use CBZ-PEG and GSF-PEG ICs as model systems for our computational analyses. In our analysis, we first calculated the binding energy, $\Delta E_{binding}$, using the DFT method. The results indicate that both CBZ-PEG IC and GSF-PEG IC exhibit relatively low $\Delta E_{binding}$, with values of -0.34 eV and -0.32 eV, respectively. These values suggest weak interactions between the host channels and the guest PEG chains (as shown in **Table 3**). To gain further insight, we conducted calculations to determine the cohesive energies ($\Delta E_{cohesive}$) of the host molecules by removing the PEG chains from the two IC structures. The $\Delta E_{cohesive}$ values for CBZ before and after optimization are -1.10 eV and -1.16 eV, respectively, with a slight decrease of -0.06 eV. This slight decrease supports the notion that CBZ channels remain relatively stable even after the removal of PEG. In contrast, for GSF channels, the optimization of the channel structure results in a more substantial energy decrease of -0.22 eV, dropping from -1.20 eV to -0.98 eV. This energy depression is significantly larger than what is observed in the CBZ system, highlighting that PEG has a much more pronounced effect on the stability of GSF channels compared to CBZ channels.

Table 3. $\Delta E_{binding}$ and $\Delta E_{cohesive}$ (before and after optimization) of CBZ-PEG and GSF-PEG ICs. The unit is eV.

	$\Delta E_{bingding}$	$\Delta E_{cohesive}$ (before opt.)	$\Delta E_{cohesive}$ (after opt.)
CBZ-PEG IC	-0.34	-1.10	-1.16
GSF-PEG IC	-0.32	-0.98	-1.20

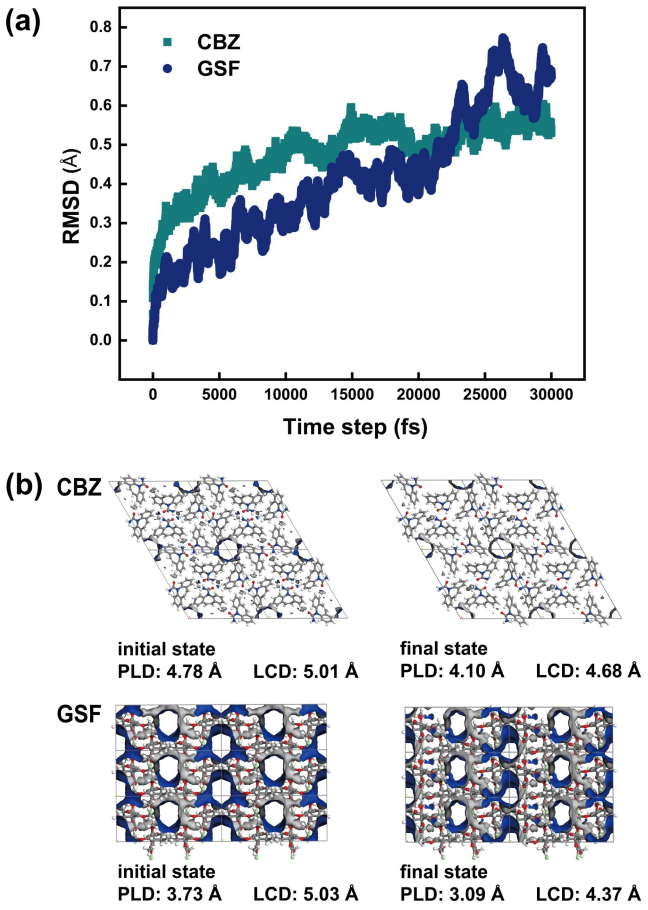

Figure 4. Molecular dynamics simulation of CBZ-PEG and GSF-PEG ICs. (a) RMSD tracks show the structural change over time after the PEG was removed. (b) Initial structure after PEG removal (left) and final structure (right) after molecular dynamics simulation for 3000 fs of CBZ (top) and GSF (below) systems.

Then, we conducted 30,000 steps of ab-initio Molecular Dynamics (AIMD) simulations on neat CBZ and GSF channels. The root mean square deviation (RMSD) values were utilized to assess changes in the structures after the removal of PEG. These RMSD values were calculated by comparing the initial structure to the structure at various time points using the molecules within a unit cell (comprising 18 molecules for CBZ and 4 molecules for GSF). As depicted in **Figure 4a**, the RMSD trajectories over time reveal that the RMSD value for CBZ channels tends to stabilize within the first 25,000 ps of the simulation. In contrast, the RMSD value for GSF channels continues to increase and exhibits strong fluctuations even after 25,000 ps. Furthermore, we examined the structural changes of CBZ and GSF channels during the dynamic simulation process and represented the results as schematic diagrams in **Figure 4b**.

The pore-limiting diameter (PLD) of the CBZ channels decreased from 4.78 Å to 4.10 Å, a reduction of 0.68 Å, which is comparable to the decrease observed in GSF channels (from 3.73 Å to 3.09 Å, a reduction of 0.64 Å). However, the largest cavity diameter (LCD) for CBZ channels only decreased by 0.33 Å, whereas the LCD for GSF channels exhibited a more significant reduction of 0.66 Å, nearly twice that of CBZ channels. This calculation result indicates that CBZ undergoes smaller structural changes after PEG removal, while GSF is more sensitive to the removal of PEG, resulting in larger changes in channel size following PEG removal.

In summary, the findings from structural analysis, DFT calculations, and MD simulations collectively validate the notion that the CBZ channel structure is inherently stable due to its unique mortise-tenon joints and strong π-π interactions. As a result, it doesn't require the insertion of guest molecules to maintain its stability. Conversely, GSF channels lack sufficient support from the relatively weak Cl...O and C-H...π intermolecular interactions, necessitating the presence of guest molecules for structural stabilization. This insight helps answer the question of why CBZ channels can exist independently in the absence of guest polymers, while GSF channels cannot.

3.4 Geometric dimensions of drug channels

Based on the dependency of channel-type structure formation on guest polymers, we suggest a classification of drug-polymer ICs into two categories. The first category is "polymer-independent ICs", where the channel structure can emerge independently, even in the absence of guest polymers. As of now, the only reported case fitting this category is CBZ-polymer IC. The second category is "polymer-dependent ICs", where the insertion of a polymer is a prerequisite for channel formation. Currently, there are seven known API cases that fall into this category, as listed in Table 4. This classification provides a useful framework for understanding the diverse behaviors of drug-polymer ICs. The fundamental distinction between the two categories of drug-polymer ICs lies in the strength of interactions between host molecules and their ability to stabilize the low-density channel structure. Currently, the majority of drug-polymer ICs fall into the second category, which is polymer-dependent. In these cases, the size of the channels is a critical parameter. They must be sufficiently large to accommodate the polymer chains. However, following the density rule[44], larger channels result in lower density and, consequently, higher energy. This can have a negative impact on the stability of the channel structure. Therefore, an important consideration is finding the right balance in channel size to both accommodate the polymer and maintain an optimal density, as these factors jointly determine the thermodynamic stability of the IC.

We calculated the channel size of eleven structurally determined drug-polymer ICs using the open-source software Zeo^{++}[38]. Structures of CBZ and GSF ICs were first determined in this work, while other structures were downloaded from CSD. The calculation results are listed in **Table 4** and **Figure 5**. Interestingly, it is observed that the channel sizes of the eleven ICs fall within a relatively narrow range of 3.86-5.18 Å. These values are slightly lower than the reported data of 5.25-5.5 Å for urea-PCL IC[45], ~4.7-5.6 Å for DIF-PCL IC[13], and ~4.6-6.5 Å for DIF-PTHF IC[13]. Interestingly, it is observed that the channel sizes of the eleven ICs fall within a relatively narrow range of 3.86-5.18 Å. These values are slightly smaller than the reported data for urea-PCL ICs (5.25-5.5 Å), DIF-PCL ICs (~4.7-5.6 Å), and DIF-PTHF ICs (~4.6-6.5 Å). What's particularly noteworthy is that different ICs of the same drug exhibit very similar channel sizes, regardless of the specific guest polymers involved. For instance, the channel sizes, as indicated by PLD values, for the three CBZ ICs and three GSF ICs are consistently within the range of 4.79-4.98 Å and 3.73-3.86 Å, respectively. This suggests that the channel size is primarily governed by the dimensions, shape, and configuration of the drug molecules, along with the intermolecular interactions between these host drugs. It is relatively unaffected by the presence of guest polymers. Consequently, a crucial condition for the formation of polymer-dependent IC is that the host molecules are capable of self-assembling into a porous structure with channels of sufficient size to accommodate the guest polymers.

Table 4. Channel size and polymer dependence of drug-polymer ICs.

Drug	Guest polymer	$T_{struc.\ det.}$ [a] (K)	PLD (Å)	LCD (Å)
Carbamazepine	PEG	100	4.79	5.02
	PCL	100	4.98	5.18
	PTHF	100	4.94	5.13
Griseofulvin	PEG	100	3.88	4.73
	PBA	100	4.14	5.08
	PES	100	3.86	4.76
Diflunisal	PCL	100 [13]	3.87	4.60
	PTHF	100 [13]	4.12	4.37
Nevirapine	PCL	100 [20]	4.07	4.77
Urea	PEG	213 [46]	4.07	4.44
Dapsone	PEG	100 [16]	3.91	4.85
Finasteride	PEG	N.A.[b]	N.A.	N.A.
Mavacoxib	PEG	N.A.	N.A.	N.A.

[a] $T_{struc.\ det.}$: The temperature at which the single-crystal structure was determined.
[b] N.A.: not available.

To qualify the relationship between the size of host channels and guest molecules, we further calculated the size of five guest polymers that have been reported to form ICs with host drugs (denoted as group 1) and four polymers that are extensively used in pharmaceutical amorphous solid dispersion (i.e. PVP, PVP VA, Soluplus and HPMC AS, denoted as group 2). Assuming the polymer chain takes on a stretched conformation, depicted as a cylindrical shape in **Figures 2-3**, we define the diameter of this cylinder as the radial diameter of the polymer. The calculation results for these radial diameter are presented in **Table 5** and visualized in **Figure 5**. Group 1 polymers have radial diameters that range from 2.83 Å to 3.50 Å. These values are lower than the PLD of ICs, which falls within the range of 3.86-4.98 Å. Conversely, Group 2 polymers feature large side groups, resulting in significantly larger radial diameters, ranging from 6.17 Å to 16.31 Å. These values surpass the PLD of previously known ICs. Perhaps due to the larger radial diameters, there have been no reports of Group 2 polymers forming ICs. To verify whether large-sized polymers could expand the channels of ICs, we conducted an experiment using GSF as a model drug and attempted to synthesize GSF-polymer ICs with

polymers from group 2 by melt crystallization. As expected, these attempts were unsuccessful. Based on these results, we can tentatively conclude that GSF channels cannot be enlarged to accommodate the large-sized polymers. This inability to expand is likely due to the fact that doing so would disrupt the intermolecular interactions that play a vital role in maintaining the structural integrity of the channels. These findings further support the previously mentioned conclusions that the size of the channels is primarily determined by the host molecules, and only polymers smaller than the channel size can effectively be inserted into these channels.

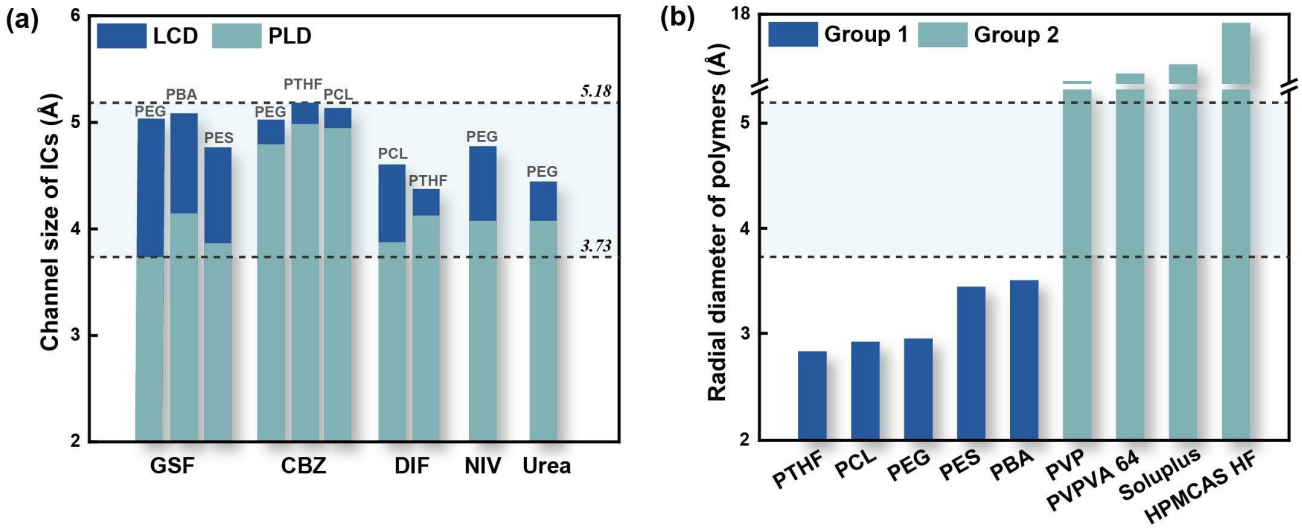

Figure 5. Channel sizes of drug-polymer ICs (a) and radical diameters of polymers (b).

Table 5. Radial diameter of polymers

	Polymer	Radial diameter (Å)	IC formation
Group 1	PTHF	2.83	Capable
	PCL	2.92	Capable
	PEG	2.95	Capable
	PES	3.44	Capable
	PBA	3.50	Capable
Group 2	PVP	6.17	Incapable
	PVPVA 64	7.47	Incapable
	Soluplus	9.09	Incapable
	HPMCAS HF	16.31	Incapable

4. Conclusions

This study underscores the significance of microdroplet melt crystallization as an effective method for the rapid synthesis of drug-polymer ICs and the efficient growth of their single crystals to facilitate structure elucidation. Thanks to this approach, we successfully determined the crystal structures of previously reported CBZ-polymer ICs and the GSF-PEG IC, in addition to two newly synthesized GSF ICs with PBA and PES. This achievement in structure identification allowed for comprehensive structural analysis and theoretical calculations, which collectively provided insight into the molecular mechanisms behind the differing dependencies of CBZ and GSF on guest polymers. In summary, we found that CBZ channels possess a unique structure where CBZ molecules with specific conformations stack into columns along the *c*-axis through π-π stacking interactions. Every six columns mechanically secure each other, forming a channel stabilized by mortise-tenon structures. Consequently, these low-density channel structures can independently form in the absence of guest molecules. In contrast, GSF channels are formed by relatively weak Cl...O and C-H...π interactions between molecules, thus necessitating the insertion of polymer chains to stabilize the channel structure. DFT calculations revealed that CBZ channels have higher cohesive energy and are therefore more stable than GSF channels. Molecular dynamics simulations further confirmed the greater stability of CBZ channels compared to GSF channels after the removal of PEG for 30,000 fs. Structural analysis and theoretical calculations collectively explain why polymer-drug ICs exhibit varying dependencies on guest polymers.

Considering the dependency of IC formation on guest polymers, we propose a classification of drug-polymer ICs into two types: polymer-independent IC (as seen in the CBZ case) and polymer-dependent IC (as exemplified by GSF). The former features a strong channel structure, while the latter presents a weaker one. Despite variations in channel formation mechanisms, it is essential for host drug molecules to have the capacity to create a porous structure with channels that can effectively accommodate the guest molecules. This serves as one of the prerequisites for IC formation. Interestingly, the channel size in currently known drug-polymer IC structures is distributed within the range of 3.86-5.18 Å. This raises further questions such as why the channel sizes fall within this narrow range, whether drugs with channel-type solvates of similar pore sizes can form drug-polymer ICs, and what additional conditions are necessary for IC formation beyond size matching. Although these issues are beyond the scope of this work, we believe that our findings, in conjunction with the application of microdroplet melt crystallization for the rapid synthesis and efficient single-crystal growth of drug-polymer ICs, will encourage further research to

explore the answers to these questions. This collective effort will promote a deeper understanding of the formation mechanisms of drug-polymer ICs and ultimately benefit the realization of theoretical prediction and practical application in the field of pharmaceuticals.

Conflicts of interest

There are no conflicts to declare.

Acknowledgements

This work was financially supported by the Guangdong Basic and Applied Basic Research Foundation (Nos. 2020A1515010782 and 2022A1515010393) and the Guangzhou Basic and Applied Basic Research Foundation (No. 202102080327). Changrui Li is grateful to the National Young Talent Program for supporting his research work in Sun Yat-sen University.

Author contributions

B.L., S.L, X.O. and A.L. performed crystallization experiments. C.L. and P.C. performed theoretical calculations. B.L., C.L. and M.L. wrote the original manuscript. P.C. and M.L. revised the manuscript and managed the project. All members participated in data analysis and discussion.

References

1. Alqahtani, M. S., Kazi, M., Alsenaidy, M. A. *et al*. Advances in oral drug delivery. *Frontiers in Pharmacology* **2021,** *12* : 618411.

2. Pindelska, E., Sokal, A., Kolodziejski, W. Pharmaceutical cocrystals, salts and polymorphs: Advanced characterization techniques. *Advanced Drug Delivery Reviews* **2017**, *117,* 111-146.

3. Cid-Samamed, A., Rakmai, J., Mejuto, J. C. *et al*. Cyclodextrins inclusion complex: Preparation methods, analytical techniques and food industry applications. *Food chemistry* ***2022*****,** *384* : 132467.

4. Araj, S. K., Szeleszczuk, Ł. A review on cyclodextrins/estrogens inclusion complexes. *International Journal of Molecular Sciences* **2023**, *24*(10): 8780

5. Szejtli, J., Past, present and futute of cyclodextrin research. *Pure and Applied Chemistry* **2004,** *76* (10), 1825-1845.

6. Suehiro, K., Nagano, Y. Structural studies on molecular complexes of polyethers, 1. Urea-ethylene oxide oligomer complexes. *Die Makromolekulare Chemie: Macromolecular Chemistry and Physics* **1983,** *184* (3), 669-674.

7. Allegra, G., Farina, M., Immirzi, A. *et al*. Inclusion compounds in perhydrotriphenylene. Part I. The crystal structure of perhydrotriphenylene and of some inclusion compounds. *Journal of the Chemical Society B: Physical Organic* **1967**, 1020-1028.

8. Allcock, H. R., Siegel, L. A. Phosphonitrilic compounds. III.1 molecular inclusion compounds of tris(o-phenylenedioxy)phosphonitrile trimer. *Journal of the American Chemical Society* **1964,** *86* (23), 5140-5144.

9. Suehiro, K., Urabe, A., Yoshitake, Y. *et al*. Structural studies on molecular complexes of polyethers, 3. Urea-polyether complexes. *Die Makromolekulare Chemie: Macromolecular Chemistry and Physics* **1984,** *185* (11), 2467-2473.

10. Sun C C. Novel co-crystals between polyethylene glycols and 5-phenylpyrazolyl-1-benzenesulfonamides. Patent WO2006024930A1. 2006.

11. Zhong, Z., Guo, C., Chen, L. *et al*. Co-crystal formation between poly(ethylene glycol) and a small molecular drug griseofulvin. *Chemical Communications* **2014,** *50* (48), 6375-8.

12. Yang, X., Zhong, Z., Huang, Y. The effect of PEG molecular weights on the thermal stability and dissolution behaviors of griseofulvin-PEG crystalline inclusion complexes. *International journal of pharmaceutics* **2016,** *508* (1-2), 51-60.

13. Zhong, Z., Guo, C., Yang, X. *et al*. Drug molecule diflunisal forms crystalline inclusion complexes with multiple types of linear polymers. *Crystal Growth & Design* **2016,** *16* (3), 1181-1186.

14. Zhong, Z., Yang, X., Fu, X. B. *et al*. Crystalline inclusion complexes formed between the drug diflunisal and block copolymers. *Chinese Chemical Letters* **2017,** *28* (6), 1268-1275.

15. Zhong, Z., Yang, X., Guo, B. H. *et al*. Dissolution behavior of the crystalline inclusion complex formed by the drug diflunisal and poly(ε-caprolactone). *Crystal Growth & Design* **2016,** *17* (1), 355-362.

16. Chappa, P., Maruthapillai, A., Voguri, R. *et al*. Drug–polymer co-crystals of dapsone and polyethylene glycol: An emerging subset in pharmaceutical co-crystals. *Crystal Growth & Design* **2018,** *18* (12), 7590-7598.

17. Zhong, Z., Yang, X., Wang, B. H. *et al*. Solvent-polymer guest exchange in a carbamazepine inclusion complex: Structure, kinetics and implication for guest selection. *CrystEngComm* **2019,** *21* (13), 2164-2173.

18. Chen, L., Huang, Y. The guest polymer effect on the dissolution of drug-polymer crystalline inclusion complexes. *RSC Advances* **2021,** *11* (22), 13091-13096.

19. Katrajkar, K., Thakkar, S., Kshirsagar, B. *et al*. Development and evaluation of crystalline inclusion complex of finasteride using electrospraying as a novel approach. *Journal of Drug Delivery Science and Technology* **2020,** *59* : 101887.

20. Yang, X., Yu, B., Zhong, Z. *et al*. Nevirapine-polycaprolactone crystalline inclusion complex as a potential long-acting injectable solid form. *International journal of pharmaceutics* **2018,** *543* (1-2), 121-129.

21. Ye, H. M., Li, H. F., Wang, C. S. *et al*. Degradable polyester/urea inclusion complex applied as a facile and environment-friendly strategy for slow-release fertilizer: Performance and mechanism. *Chemical Engineering Journal* **2020,** *381* : 122704.

22. Yang, X., Zhong, Z., Xu, J. *et al*. Drug-polymer inclusion complex as a new pharmaceutical solid form. *Chinese Chemical Letters* **2017,** *28* (11), 2099-2104.

23. Saha, A., Nia, S. S., Rodríguez, J. A. Electron diffraction of 3D molecular crystals. *Chemical Reviews* **2022,** *122* (17), 13883-13914.

24. Ou, X., Li, X., Rong, H. *et al*. A general method for cultivating single crystals from melt microdroplets. *Chemical Communications* **2020,** *56* (69), 9950-9953.

25. Ou, X., Li, S., Chen, Y. *et al*. Polymorphism in griseofulvin: New story between an old drug and polyethylene glycol. *Crystal Growth & Design* **2022,** *22* (6), 3778-3785.

26. Li, X., Ou, X., Wang, B. *et al*. Rich polymorphism in nicotinamide revealed by melt crystallization and crystal structure prediction. *Communications Chemistry* **2020,** *3*(1): 152.

27. Lightowler, M., Li, S., Ou, X. *et al*. Indomethacin polymorph δ revealed to be two plastically bendable crystal forms by 3d electron diffraction: Correcting a 47-year-old misunderstanding. *Angewandte Chemie International Edition* **2021**, *134*(7): e202114985.
28. Ao, L., Shuting, L., Jiashu, W. *et al*. Pterostilbene–nicotinamide cocrystal: A case report of single cocrystals grown from melt microdroplets. *Crystal Growth & Design* **2022**, *23*(1), 6-10.
29. Chaudhary, A., Nagaich, U., Gulati, N. *et al*. Enhancement of solubilization and bioavailability of poorly soluble drugs by physical and chemical modifications: *Journal of Advanced Pharmacy Education and Research.* **2012,** *2* (1), 32-67.
30. Cruz Cabeza, A. J., Day, G. M., Motherwell, W. D. *et al*. Solvent inclusion in form II carbamazepine. *Chemical Communications* **2007,** *16*, 1600-1602.
31. Aitipamula, S., Chow, P. S., Tan, R. B. Solvates of the antifungal drug griseofulvin: Structural, thermochemical and conformational analysis. *Crystal Engineering and Materials,* 2014, *70*(1), 54-62.
32. Rigaku, O. CrysAlis PRO Software system. Rigaku Corporation. Oxford, UK: 2018.
33. Sheldrick, G. M. SHELXT–Integrated space-group and crystal-structure determination. *Acta Crystallographica Section A: Foundations and Advances* **2015,** *71*(1), 3-8.
34. Sheldrick, G. M., Crystal structure refinement with SHELXL. *Acta Crystallographica Section C: Structural Chemistry* **2015,** *71*(1), 3-8.
35. Kresse, G., Furthmüller, J. Efficient iterative schemes for ab initio total-energy calculations using a plane-wave basis set. *Physical review. B, Condensed matter* **1996,** *54* (16), 11169-11186.
36. Perdew, J. P., Burke, K., Ernzerhof, M. Generalized gradient approximation made simple. *Physical review letters* **1996,** *77* (18), 3865-3868.
37. Blöchl, P. E. Projector augmented-wave method. *Physical review. B, Condensed matter* **1994,** *50* (24), 17953-17979.
38. Willems, T. F., Rycroft, C. H., Kazi, M. *et al*. Algorithms and tools for high-throughput geometry-based analysis of crystalline porous materials. *Microporous and Mesoporous Materials* **2012,** *149* (1), 134-141.
39. Nievergelt, P. P., Spingler, B. Growing single crystals of small molecules by thermal recrystallization, a viable option even for minute amounts of material? *CrystEngComm* **2017,** *19* (1), 142-147.
40. M. Gunn, E., A. Guzei, I., Yu, L. Does crystal density control fast surface crystal growth in glasses? A study with polymorphs. *Crystal Growth & Design* **2011,** *11* (9), 3979-3984.
41. Arlin, J. B., Price, L. S., Price, S. L. *et al*. A strategy for producing predicted polymorphs: Catemeric carbamazepine form V. Chemical Communications **2011**, *47*(25), 7074-7076.
42. Krahn, F., Mielck, J. J. P. A. H. Relations between several polymorphic forms and the dihydrate of carbamazepine. Pharmaceutica Acta Helvetiae **1987**, *62* (9), 247-254
43. D'Souza A, A., Shegokar, R. Polyethylene glycol (PEG): A versatile polymer for pharmaceutical applications. Expert opinion on drug delivery, **2016**, *13* (9), 1257-1275.
44. Hirakawa, Y., Ueda, H., Miyano, T. et al. New insight into transdermal drug delivery with supersaturated formulation based on co-amorphous system. **2019,** *569*, 118582.
45. Van Santen, R. A. The Ostwald step rule. **1984,** *88* (24), 5768-5769.
46. Lu, J., Mirau, P. A., Tonelli, A. E. Chain conformations and dynamics of crystalline polymers as observed in their inclusion compounds by solid-state NMR. **2002,** *27* (2), 357-401.